Supporting Information

Accessing the Nitromethane (CH_3NO_2) Potential Energy Surface in Methanol (CH_3OH)–Nitrogen Monoxide (NO) Ices Exposed to Ionizing Radiation: An FTIR and PI-ReTOF-MS Investigation

Sándor Góbi[1,2], Parker B. Crandall[1], Pavlo Maksyutenko[1,3], Marko Förstel[1,4], Ralf I. Kaiser[1,*]

[1] Department of Chemistry, University of Hawai'i at Mānoa, Honolulu, HI 96822, USA
W.M. Keck Laboratory in Astrochemistry, University of Hawai'i at Mānoa, Honolulu, HI 96822, USA
[2] Present address: Department of Chemistry, University of Coimbra, 3004-535, Coimbra, Portugal
[3] Present address: Harvard-Smithsonian Center for Astrophysics, 60 Garden Street, Cambridge, MA, 02138, USA
[4] Present address: Berlin Institute of Technology, IOAP, Hardenbergstrasse 36, 10623 Berlin, Germany
ralfk@hawaii.edu

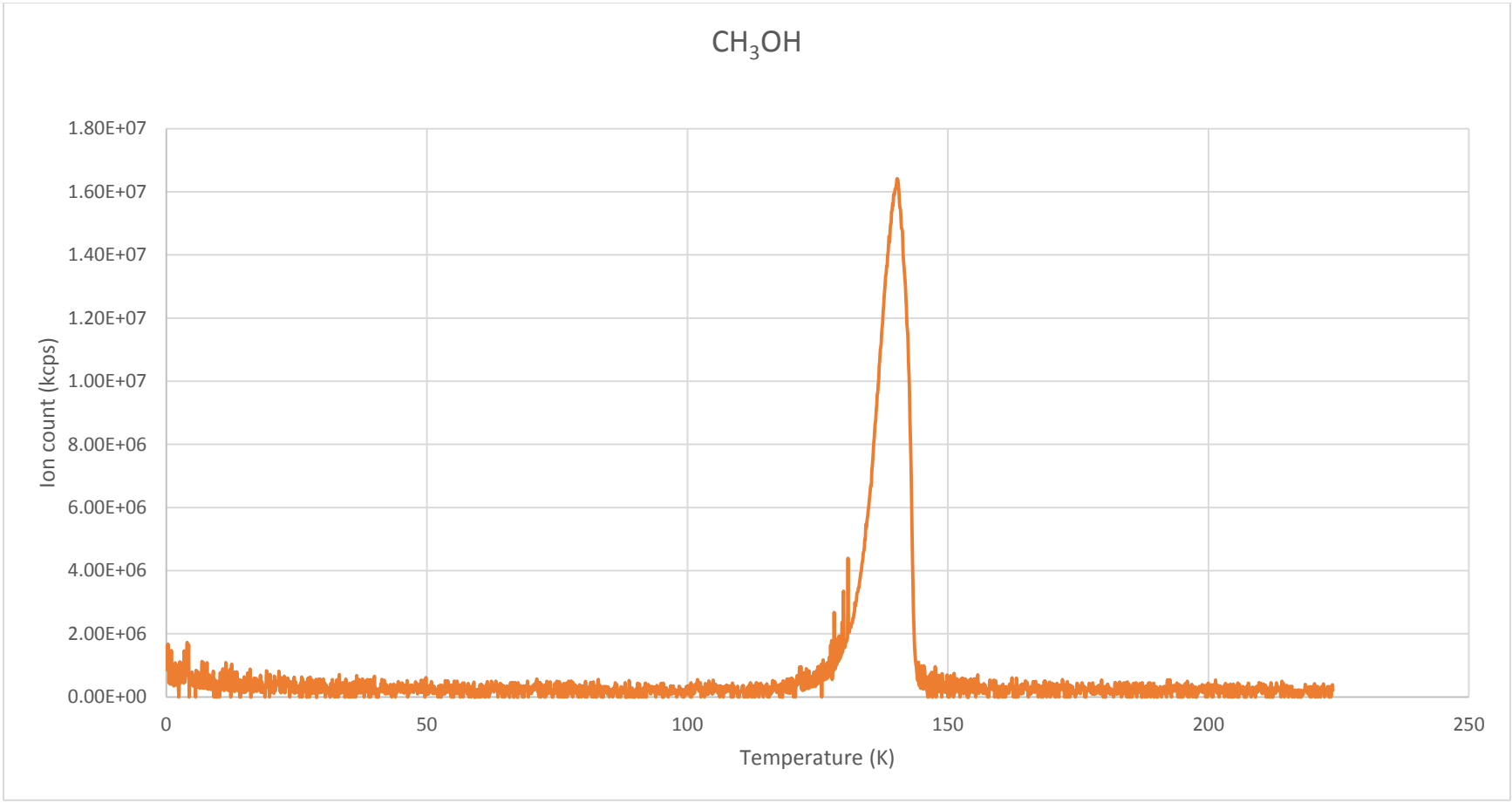

Figure S1. Calibration EI-QMS TPD curve of 1 fringe of neat CH_3OH ice deposited on a silver substrate at 5.5 K.

Table S1. Physical quantities connected to the CH_3OH ice.

Physical quantity	Value
Refractive index	1.3284
Thickness (nm)	240
Density (g cm^{-3})	1.02
Mass (g)	2.43×10^{-5}
Molar mass (g mol^{-1})	32.04
Amount (mol)	7.59×10^{-7}
Avogadro's number	6.02×10^{23}
Number of molecules	4.57×10^{17}
Integrated EI-QMS signal (kcps)	1.36×10^{9}
Conversion factor	3.37×10^{8}

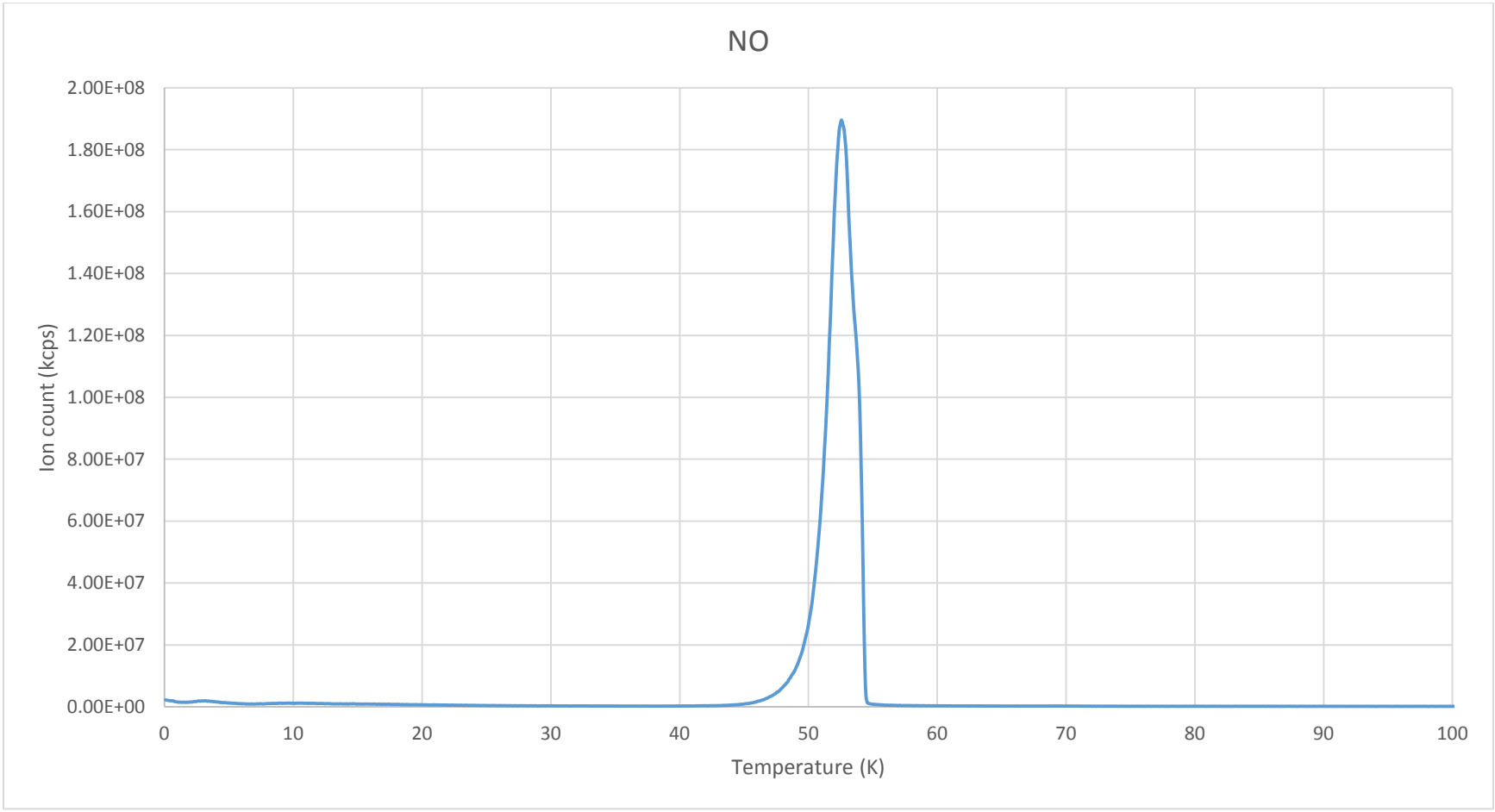

Figure S2. Calibration EI-QMS TPD curve of 1 fringe of neat NO ice deposited on a silver substrate at 5.5 K.

Table S2. Physical quantities connected to the NO ice.

Physical quantity	Value
Refractive index	1.22
Thickness (nm)	260
Density (g cm^{-3})	1.25
Mass (g)	3.25×10^{-5}
Molar mass (g mol^{-1})	30.01
Amount (mol)	1.08×10^{-6}
Avogadro's number	6.02×10^{23}
Number of molecules	6.52×10^{17}
Integrated EI-QMS signal (kcps)	5.52×10^{9}
Conversion factor	1.18×10^{8}

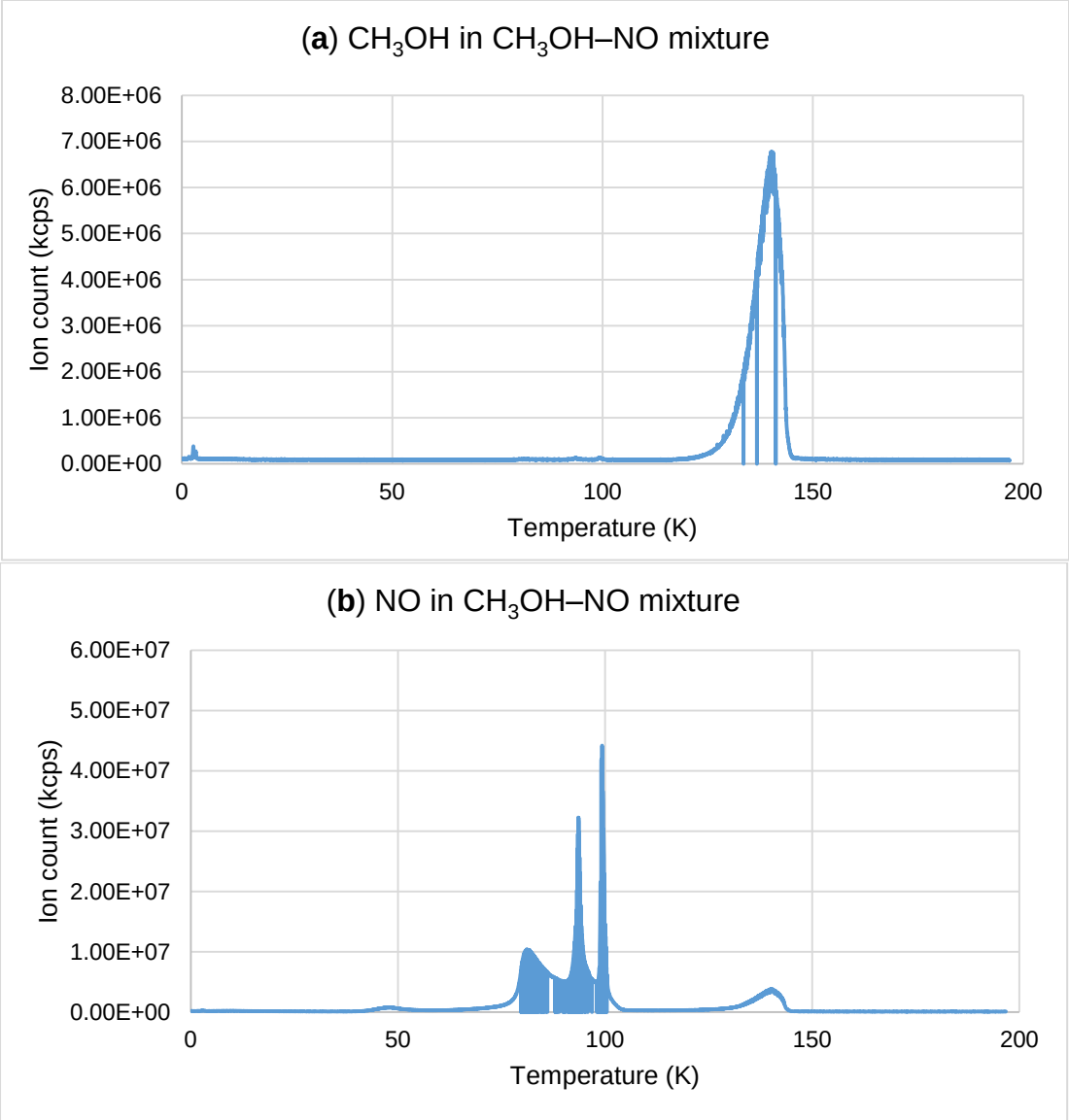

Figure S3. Calibration EI-QMS TPD curve of 2 fringes of (**a**) CH_3OH, (**b**) NO in a CH_3OH–NO ice mixture deposited on a silver substrate at 5.5 K.

Table S3. Physical quantities connected to the CH_3OH–NO ice mixture.

Physical quantity	Value
Refractive index	1.16[a]
Thickness (nm)	540[b] / 540[c]
Average density (g cm^{-3})[a]	1.12
Mass (g)	2.85×10^{-5} [d] / 3.23×10^{-5} [e]
Average molar mass (g mol^{-1})[a]	30.93
Amount of substances (mol)	8.90×10^{-7} [d] / 1.08×10^{-6} [e]
Avogadro's number	6.02×10^{23}
Number of molecules	5.36×10^{17} [d] / 6.48×10^{17} [e]
Integrated EI-QMS signal (kcps)	1.59×10^{9} [d] / 5.49×10^{9} [e]
Ratio[b]	$1.2 \pm 0.1 : 1.0$

[a] Calculated by using the equations shown in Figure S7.

[b] Calculated from calibrated EI-QMS signals.

[c] Calculated from laser interferometry.

[d] CH_3OH

[e] NO

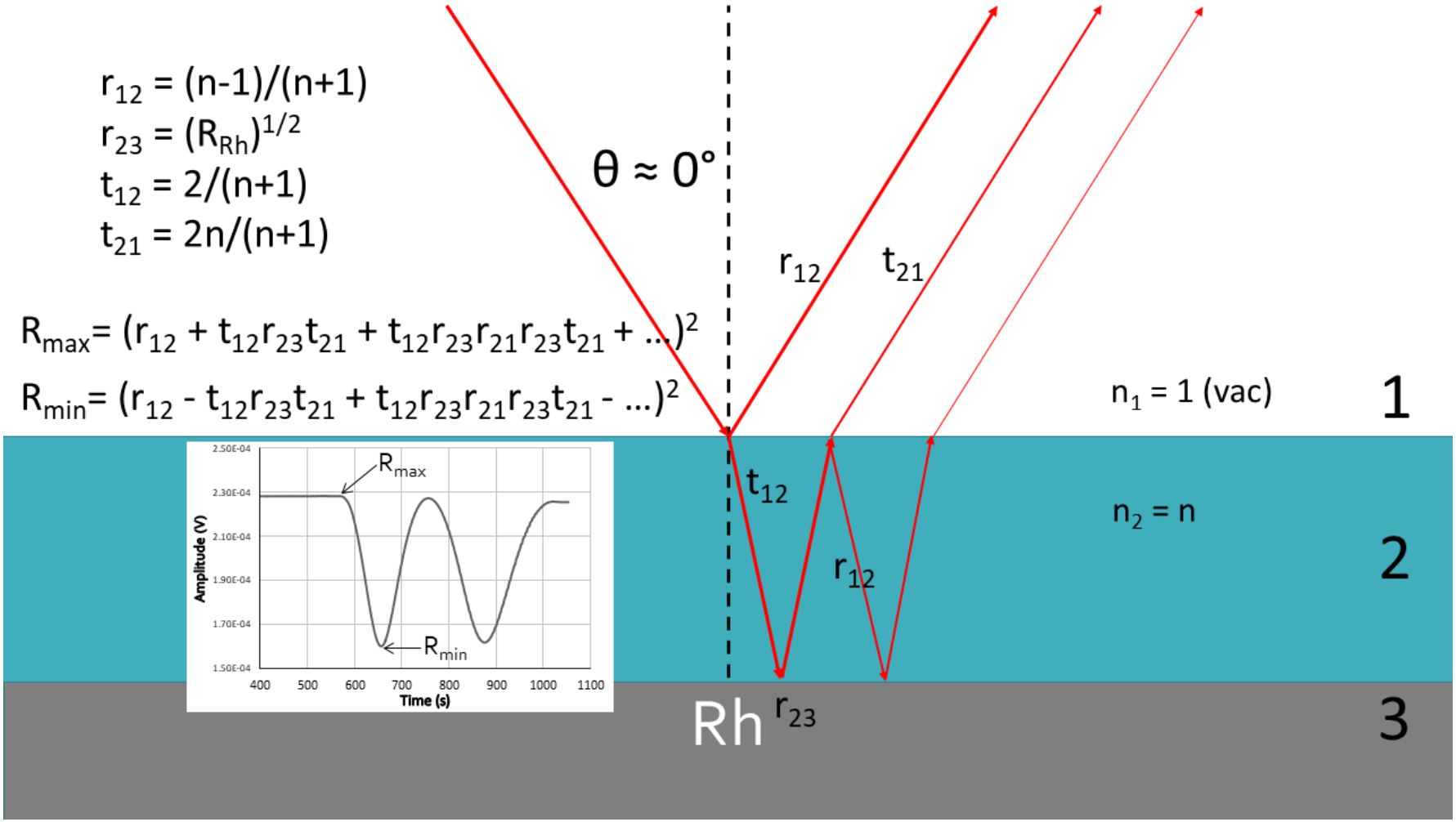

Figure S4. Equations used to calculate the refractive index of the CH_3OH–NO ice mixture.[1]

Table S4. Summary of the electron irradiation experiments of neat NO, CH_3OH, and CD_3OH ices at 5.5 K**.**

Ice	NO	CH_3OH	CD_3OH
Average molar mass of the ice, M (g mol^{-1})	30.01	32.04	35.06
Average density of the ice, ρ (g cm^{-3})[a]	1.22	1.02	1.12
Irradiated area, A (cm^2)	1.0 ± 0.1	1.0 ± 0.1	1.0 ± 0.1
Angle of incidence, θ (^{o})	70	70	70
Irradiation time, t (s)	3600 ± 2	3600 ± 2	3600± 2
Applied electron current, I (nA)	15 ± 2	15 ± 2	15 ± 2
Total number of electrons generated (×10^{14})	3.4 ± 0.3	3.4 ± 0.3	3.4 ± 0.3
Initial kinetic energy of the electrons, E_{init} (keV)	5.0	5.0	5.0
Average kinetic energy of backscattered electrons, E_{bs} (keV)[b]	3.4 ± 0.1	3.2 ± 0.1	3.2 ± 0.1
Fraction of backscattered electrons, f_{bs} (%)[b]	39 ± 2	33 ± 2	33 ± 2
Average kinetic energy of transmitted electrons, E_{trans} (keV)[b]	0.0 ± 0.0	0.0 ± 0.0	0.0 ± 0.0
Fraction of transmitted electrons, f_{trans} (%)[b]	0.0 ± 0.0	0.0 ± 0.0	0.0 ± 0.0
Simulated average penetration depth, l (nm)[b]	270 ± 10	260 ± 10	240 ± 10
Total number of molecules exposed (×10^{17})	6.5 ± 0.7	5.0 ± 0.5	4.5 ± 0.5
Dose per molecule, D (eV)	1.9 ± 0.3	2.7 ± 0.4	2.9 ± 0.4

[a] As the density values for the deuterated species is not available, it was assumed that the same number of molecules occupies equal volume for both the CH_3OH and CD_3OH samples.

[b] Values from CASINO simulations.

VUV generation details

10.20 eV (121.6 nm) VUV light was generated by resonant four-wave mixing ($\omega_{VUV} = 2\omega_1 - \omega_2$) in 1.5×10^{-4} Torr of krypton (99.999%, Specialty Gases of America) as the nonlinear medium. In order to do this, 606.948 nm (2.04 eV) light was produced by the first dye laser (Sirah Lasertechnik, Cobra-Stretch) using a mixture of Rhodamine 640 and Rhodamine 610 dyes (Exciton). This was pumped by the second harmonic of the fundamental of an Nd:YAG laser (532 nm, 2.33 eV, Spectra Physics, PRO-270-30) and tripling the dye laser output frequency using β-BaB_2O_4 (BBO) crystals (44° and 77°). This resulted in ω_1 to be 6.13 eV (202.3 nm), which were mixed with ω_2 = 2.05 eV (604.80 nm) light that was generated by the second dye laser (Sirah Lasertechnik, PrecisionScan) using a mixture of Rhodamine 640 and Rhodamine 610 dyes. The second dye laser was pumped by the second harmonic of the fundamental of the second Nd:YAG laser.

Krypton was utilized as well to obtain VUV photons with an energy of 9.80 eV (126.5 nm). For this, mixing ω_1 = 6.13 eV (202.3 nm) photons with ω_2 = 2.46 eV (504.00 nm) photons generated by the second dye laser using Coumarin 503 (Exciton) dye was done.

Xenon was necessary as a nonlinear medium to generate the 9.15 eV (135.50 nm) photoionization energy, which needed the third harmonic of the first Nd:YAG laser (355 nm, 3.49 eV). This pumped the first dye laser using Coumarin 450 dye to produce 445.132 nm (2.79 eV), which was frequency doubled to obtain ω_1 = 5.57 eV (222.66 nm). Then it was mixed with ω_2 = 1.99 eV (623.04 nm) VUV photons generated by using a mixture of Rhodamine 640 and Rhodamine 610 in the second dye laser pumped by the second harmonic of the fundamental of the second Nd:YAG laser. The generated VUV light was then separated by the LiF biconvex lens and directed to the main chamber.

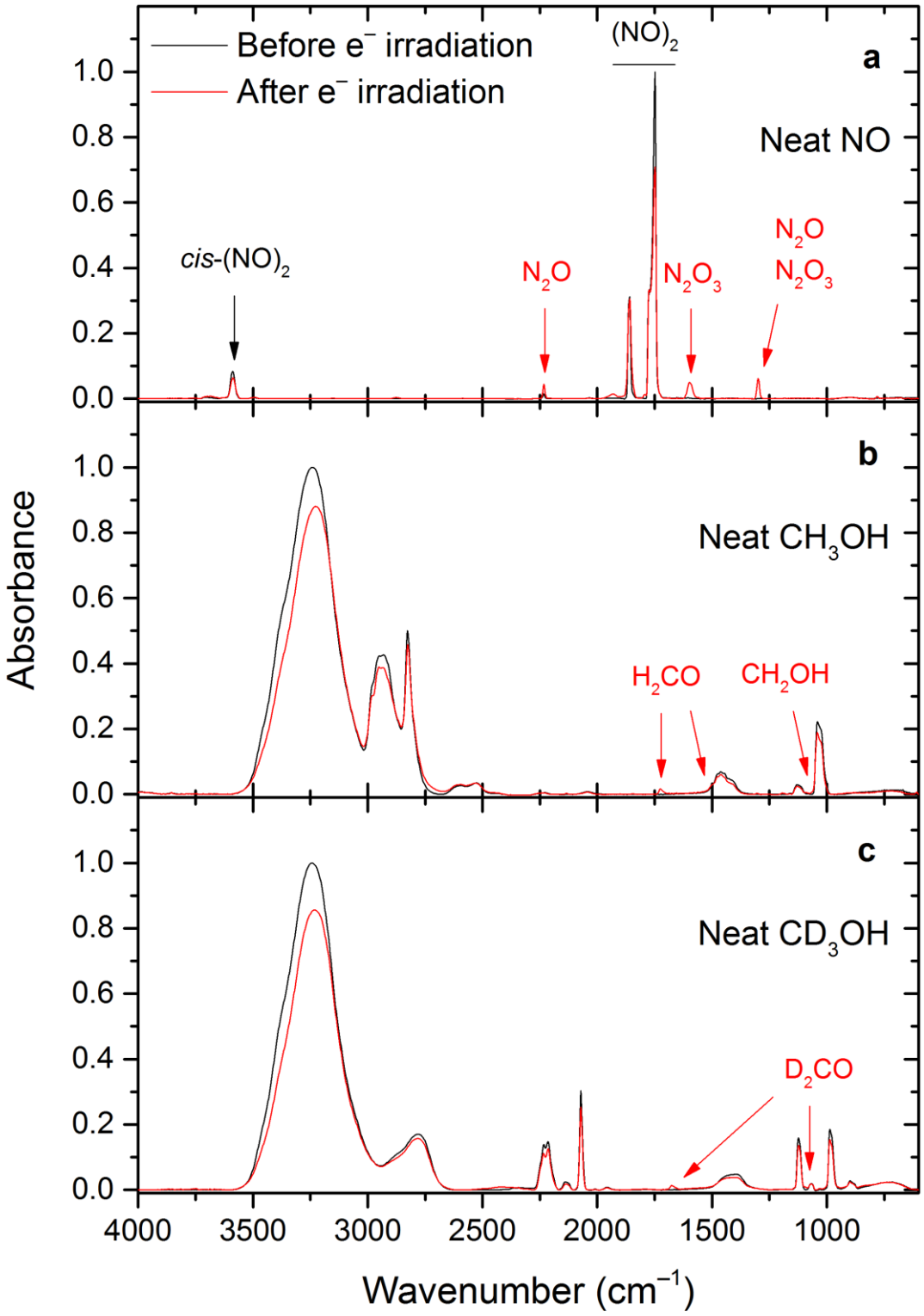

Figure S5. FTIR spectra of neat (**a**) NO, (**b**) CH_3OH, and (**c**) CD_3OH ices before (black) and after irradiation (red).

Table S5. Assignment of the FTIR data of the neat NO ice electron irradiation experiment.[a]

Wavenumber (cm^{-1})[b] Before irrad.	After irrad.	Change upon irrad.[c]	Vibr. mode	Assignment[d]	Reference
3588m	3588m	–	$\nu_1 + \nu_5$	*cis*-$(NO)_2$	2
2232w	2232m	+	ν_1	νN≡N **(N_2O)**	3
1860s	1860m	–	ν_1	ν_sN=O (*cis*-$(NO)_2$)	
	1847sh	+	ν_1	νN=O **(N_2O_3)**	
1775sh, 1749vs	1775s, 1749vs,b	–	ν_5	ν_{as}N=O (*cis*-$(NO)_2$)	4, 5
–	1597m	+	ν_2	$\nu_{as}NO_2$ **(N_2O_3)**	
–	1299m	+	ν_3	$\nu_s NO_2$ **(N_2O_3)**	
–	1287sh	+	ν_3	νN–O **(N_2O)**	3
780vw	780w	+	ν_4	βNO_2 **(N_2O_3)**	4, 5

[a] Radiolysis products are highlighted in bold.

[b] vs, very strong; s, strong; m, medium; w, weak; vw, very weak; sh, shoulder; b, broad; −, no signal

[c] −/+, decrease/increase of signal; b, broadening upon irradiation

[d] ν: stretching, β: bending, s: symmetric, as: antisymmetric vibrations

Table S6. Assignment of the FTIR data of the neat CD_3OH ice electron irradiation experiment.[a,b]

Wavenumber (cm^{-1})[c] Before irrad.	After irrad.	Change upon irrad.[d]	Vibr. mode	Assignment[e]	Reference
3377sh, 3230vs	3377sh, 3230vs	–, b	ν_1	νO–H (CD_3OH)	6,7
2877sh, 2783s,b	2877sh, 2783s,b	–, b	$2\nu_6$	2βO–H (CD_3OH)	7
2233m, 2214m	2233m, 2214m	–	ν_2, ν_9	$\nu_{as}CD_3$ (CD_3OH)	6,7
2140w	2140w	–	$2\nu_{10}$	$2\beta_{as}CD_3$ (CD_3OH)	7
2070s	2070s	–	ν_3	ν_sCD_3 (CD_3OH)	6,7
2009vw	2009vw	–	$2\nu_4$	$2\beta_{as}CD_3$ (CD_3OH)	7
1958vw	1958vw	–	$2\nu_8$	2νC–O (CD_3OH)	7
–	1676vw	+	ν_2	νC=O **(D_2CO)**	8
1414m,b	1414m,b	–, b	ν_6	βOH (CD_3OH)	6,7
–	1220vw,b	+	ν_6	νC–O **(CD_2OH)**	8,9
1123s	1123m	–, b	ν_5	β_sCD_3 (CD_3OH)	6,7
–	1099sh	+	ν_3	βCD_2 **(D_2CO)**	8
1067w	1067w	–			
1033vw, 1028vw	1032vw	+[f], b	ν_4, ν_{10}	$\beta_{as}CD_3$ (CD_3OH)	6,7
987s	987s	–	ν_8	νC–O (CD_3OH)	6,7
–	949sh	+	ν_6	ωCD_2 **(D_2CO)**	8
898w, 880sh	898w, 880sh	–	ν_7, ν_{11}	ρCD_3 (CD_3OH)	6,7

[a] For the assignment of electron irradiated CH_3OH ices, see reference 10.

[b] Radiolysis products are highlighted in bold.

[c] vs, very strong; s, strong; m, medium; w, weak; vw, very weak; sh, shoulder; b, broad; −, no signal

[d] –/+, decrease/increase of signal; b, broadening upon irradiation

[e] ν: stretching, β: bending, ρ: rocking, ω: wagging, s: symmetric, as: antisymmetric vibrations

[f] Increase in signal strength due to overlapping with the ν_6 vibrational mode of the forming CD_3H product molecule.

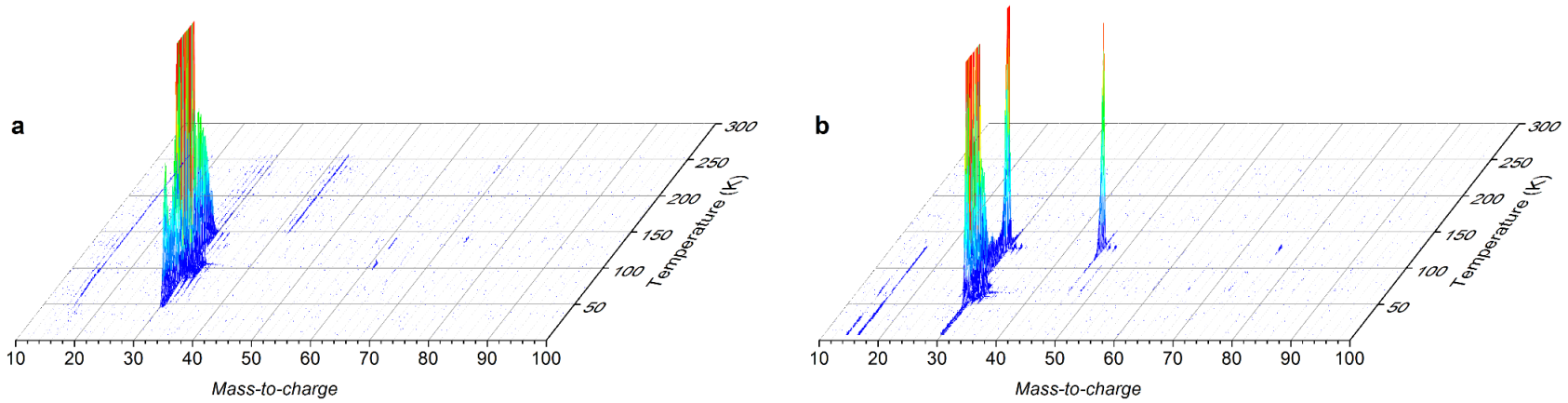

Figure S6. Three-dimensional visualization of the PI-ReTOF-MS data of the (**a**) blank and (**b**) irradiated neat NO ice samples at the photoionization energy of 10.49eV.

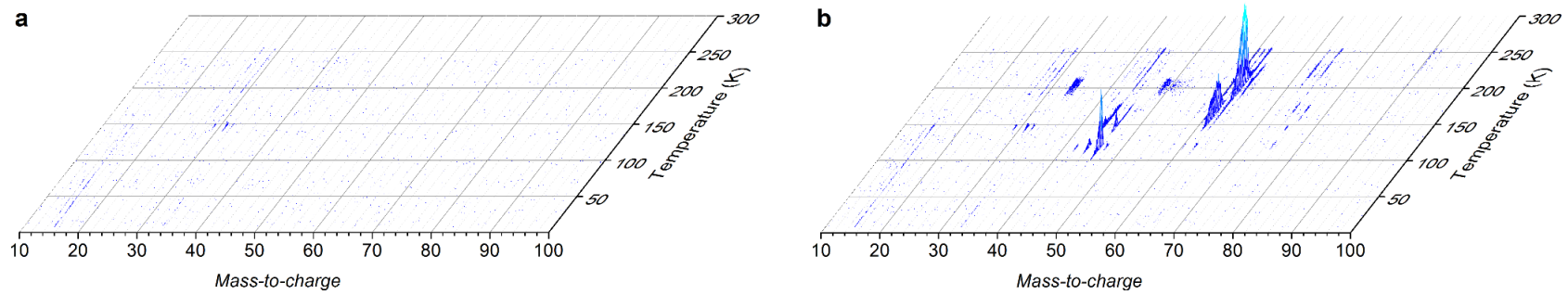

Figure S7. Three-dimensional visualization of the PI-ReTOF-MS data of the (**a**) blank and (**b**) irradiated neat CH_3OH ice samples at the photoionization energy of 10.49eV.

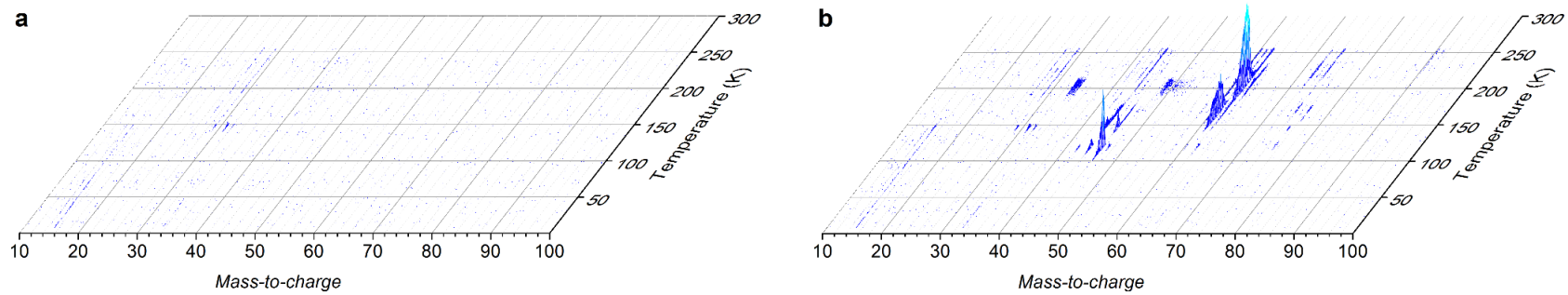

Figure S8. Three-dimensional visualization of the PI-ReTOF-MS data of the (**a**) blank and (**b**) irradiated neat CD_3OH ice samples at the photoionization energy of 10.49eV.

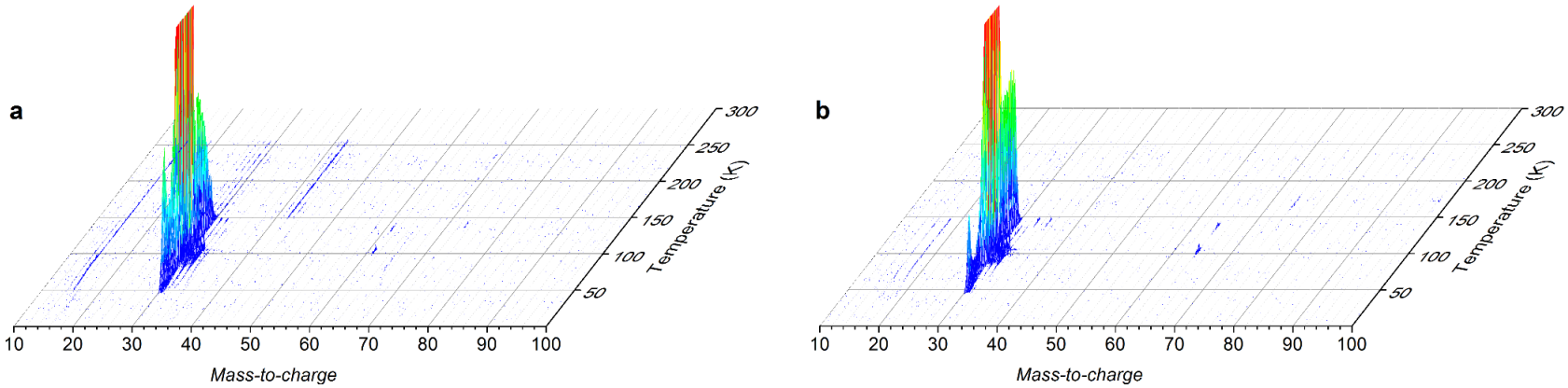

Figure S9. Three-dimensional visualization of the PI-ReTOF-MS data of the blank (**a**) CD_3OH–NO and (**b**) CD_3OH–NO ice samples at the photoionization energy of 10.49eV.

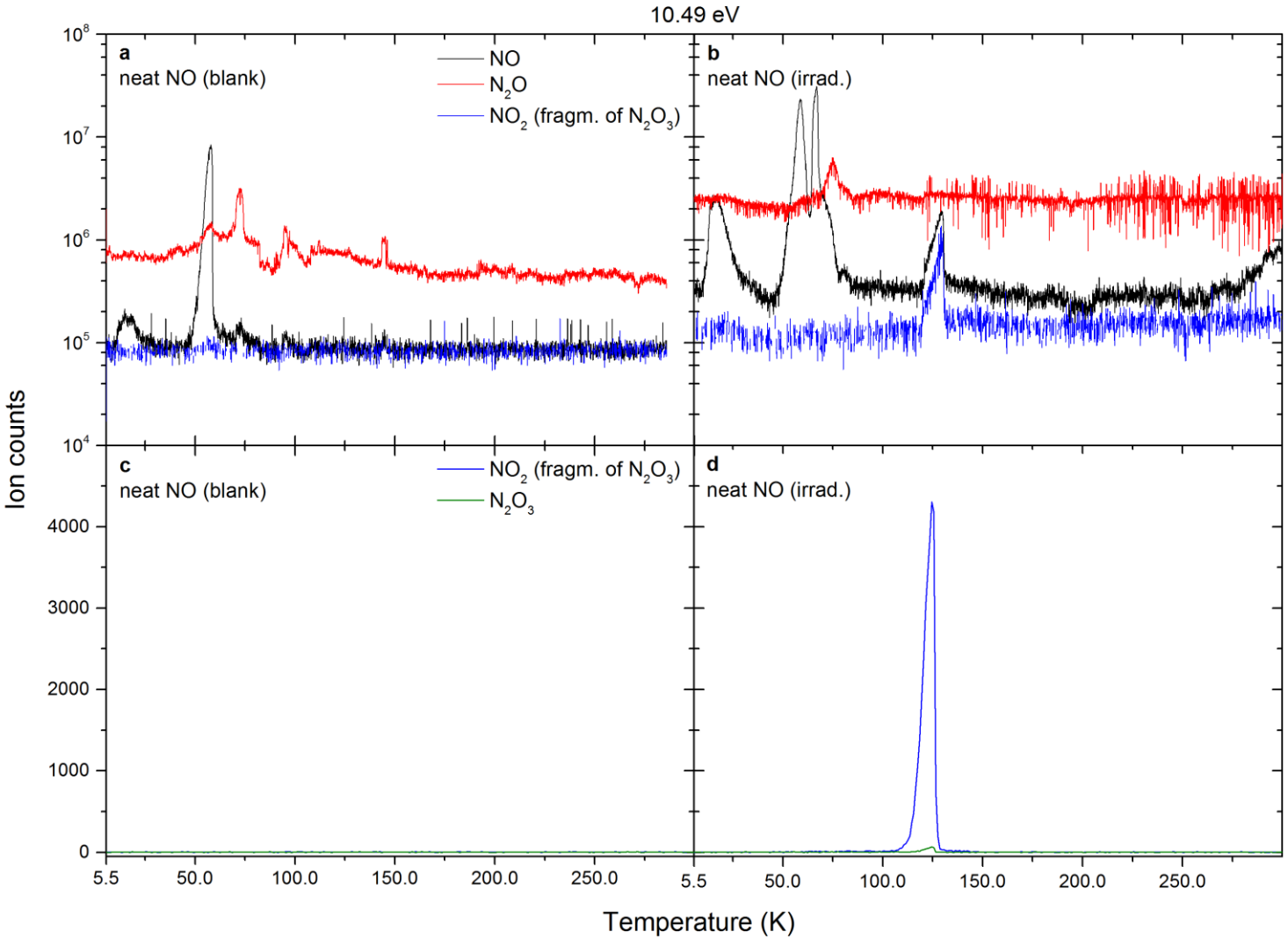

Figure S10. EI-QMS data of selected species subliming from the (**a**) blank and (**b**) irradiated neat NO ices. Data in (**c**) and (**d**) show the respective PI-ReTOF-MS profiles at the photoionization energy of 10.49eV.

Table S7. Signals detected by the PI-ReTOF-MS technique in the irradiated neat NO ice at the photoionization energy of 10.49 eV.

m/z	Species	Fragment of	$T_{sublim.}$ (K)	*IE* (eV)	References
76	N_2O_3	–	127	N/A	–
46	NO_2	N_2O_3	127	N/A	–
30	$^{14}N^{16}O$[a]	N_2O_3,	127,	N/A,	–
		N_2O (co-subl.),	75,	N/A,	–
		$(NO)_2$ (co-subl.?),	66,	N/A,	–
		–	59	9.2643 ± 0.0002	11

[a] Isotopologues at *m/z* = 31, 32, 33 can be observed as well.

Table S8. Signals detected by the PI-ReTOF-MS technique in the irradiated neat CD_3OH ice at the photoionization energy of 10.49 eV.[a]

m/z	Species	$T_{sublim.}$ (K)	IE (eV)	References
96	CD_3OCD_2OCDO	256	?	–
95	$CD_3OC(O)CD_2OH$	255	10.42	12
94	$HOCD_2CD(OH)CDO$	257	?	–
	$HOCD_2C(O)CD_2OH$		?	
84	$CD_3OC_3D_7$	174	?	–
	$C_2D_5OC_2D_5$		?	
83	$CD_3(CD_2)_3OH$	171	9.99 ± 0.05	13
	$CD_3CD_2CD(OH)CD_3$		9.88 ± 0.03	
	$(CD_3)_2CDCD_2OH$		10.02 ± 0.05	
	$(CD_3)_3COH$		9.90 ± 0.03	
	$CD_3O(CD_2)OH$		?	
	$C_2D_5OCD_2OH$		?	
80	C_3D_7CDO	221, 244	9.83	14
	$(CD_3)_2CDCDO$		9.72	14
	$C_2D_5C(O)CD_3$		9.52	15
	$CD_3C(O)OCD_3$	175	10.25	16
	$CD_3(CD)_2CD_2OH$	219	9.13	14
79	$CD_3C(O)CD_2OH$	177, 245	10.0 ± 0.1	17
	$CD_3CD(OH)CDO$		?	–
	$HO(CD_2)CDO$		?	–
76	C_2D_5COOH	223	10.51	15
	$CD_3C(O)CDO$		9.6	12
	$ODCCD_2CDO$		?	–
75	$ODCC(OH)CD_2$	229	?	–
	$HO(CD)_2CDO$		?	
68	$C_3D_4O_2$[b]	256	?	–
	$C_2D_5OCD_3$	122, 148, 171, 207	9.72 ± 0.07	18

67	C_3D_7OH $(CD_3)_2CDOH$	171, 207	10.22 ± 0.04 10.12 ± 0.03	19
66	$HO(CD_2)_2OH$	171, 206	10.16	**Error! Reference source not found.**
65	$C_2D_4HO_2$[c]	170, 205, 248	?	–
64	C_2D_5CDO CD_3COCD_3	207, 248	9.96 9.695 ± 0.006[d]	15 21
	$C_2D_4O_2$?[c], C_4D_8[e]	170	?	–
63	$HOCD_2CDO$ $CD_2=CDCD_2OH$ C_3D_5HO isomers	205, 223 174, 186	10.2 9.67 ± 0.05 ?	12 22
62	$HO(CD)_2OH$	208	9.62 ± 0.04	23
52	CD_3OCD_3	120, 148	10.025 ± 0.025	24
51	C_2D_5OH	121, 151	10.47 ± 0.02	19
48	CD_3CDO	121, 149	10.22 ± 0.01	25
47	$CD_2=CDOH$	120, 151, 171, 209, 244	9.33 ± 0.01	26
44	$CD_2C=O$	120, 190	9.6130 ± 0.0003[d]	27

[a] For the signals detected in the irradiated CH_3OH ice, see reference 12.

[b] Fragment of an $C_3D_6O_3$ isomer.

[c] Fragment of D_5-methoxymethanol (CD_3OCD_2OH).

[d] Photoionization energies of the deuterated species, in all other cases the *IE*s of the non-deuterated counterparts are shown due to lack of available data.

[e] Fragment of $C_4H_{10}O$ isomer.

Table S9. Mass balance of the neat NO ice as well as that of the irradiation products determined from their experimental IR Decay/Growth Curves.

Process	Decay product	# of molecules produced / decomposed during irradiation
$NO \rightarrow X$		$(5.1 \pm 1.4) \times 10^{17}$
Fraction of NO degraded		76 ± 14%
# of products in sample after irradiation	N_2O_3	$(1.5 \pm 0.6) \times 10^{16}$
	N_2O	$(3.5 \pm 0.1) \times 10^{15}$
	Nitrogen balance[a]	7 ± 5%
	Oxygen balance[a]	9 ± 6%

[a] Fraction of nitrogen or oxygen atoms originating from NO destruction that are needed for radiolysis product formation

Table S10. Mass balance of the neat CH_3OH ice as well as that of the irradiation products determined from their experimental IR Decay/Growth Curves.

Process	Decay product	# of molecules produced / decomposed during irradiation
$CH_3OH \rightarrow X$		$(4.6 \pm 0.9) \times 10^{17}$
Fraction of CH_3OH degraded		92 ± 4%
# of products in sample after irradiation	H_2CO	$(6.8 \pm 2.1) \times 10^{15}$
	CH_4	$(2.3 \pm 0.1) \times 10^{15}$
	CH_2OH	$(2.1 \pm 0.1) \times 10^{15}$
	CO	$(1.3 \pm 0.1) \times 10^{15}$
	HCO	$(1.3 \pm 0.2) \times 10^{14}$
	Carbon balance[a]	3 ± 1%
	Oxygen balance[a]	2 ± 1%

[a] Fraction of carbon or oxygen atoms originating from CH_3OH destruction that are needed for radiolysis product formation.

Table S11. Mass balance of the neat CD_3OH ice as well as that of the irradiation products determined from their experimental IR Decay/Growth Curves.

Process	Decay product	# of molecules produced / decomposed during irradiation
$CD_3OH \rightarrow X$		$(4.1 \pm 0.9) \times 10^{17}$
Fraction of CH_3OH degraded		89 ± 5%
# of products in sample after irradiation	D_2CO[a]	$(7.7 \pm 3.7) \times 10^{15}$
	CD_2OH	$(2.4 \pm 0.4) \times 10^{14}$
	Carbon balance[b]	2 ± 1%
	Oxygen balance[b]	2 ± 1%

[a] Absorption coefficients were assumed to be the same as for the normal isotopologue.

[b] Fraction of carbon or oxygen atoms originating from CD_3OH destruction that are needed for radiolysis product formation.

Table 12. Mass balance of the CD_3OH–NO system as well as that of the irradiation products determined from their experimental IR Decay/Growth Curves.[a]

Process	Decay product	# of molecules produced / decomposed during irradiation
$CD_3OH \rightarrow X$		$(2.4 \pm 0.5) \times 10^{17}$
Fraction of CD_3OH degraded		87 ± 5%
$NO \rightarrow X$		$(2.2 \pm 0.4) \times 10^{17}$
Fraction of NO degraded		71 ± 1%
# of products in sample after irradiation	*c*-CD_3ONO	$(9.0 \pm 0.1) \times 10^{16}$
	t-CD_3ONO[b]	$(8.5 \pm 0.1) \times 10^{16}$
	N_2O	$(7.0 \pm 0.6) \times 10^{15}$
	CD_3H	$(5.1 \pm 0.1) \times 10^{15}$
	D_2CO	$(3.2 \pm 0.1) \times 10^{15}$
	N_2O_3	$(1.5 \pm 0.1) \times 10^{15}$
	CD_2OH	$(8.4 \pm 0.7) \times 10^{14}$
	CO[c]	$(8.1 \pm 0.3) \times 10^{14}$
	CO_2	$(5.0 \pm 0.3) \times 10^{13}$
	Carbon balance[d]	82 ± 19%
	Oxygen balance[d]	81 ± 10%
	Nitrogen balance[d]	42 ± 6%

[a] Absorption coefficients – where absent – were assumed to be the same as for the normal isotopologues.

[b] The absorption coefficient was assumed to be the same as for the *cis* isomer.

[c] The column density of CO was assumed to be the same as for the CD_3OH–NO mixture sample.

[d] Fraction of carbon atoms originating from CD_3OH or oxygen/nitrogen atoms from CD_3OH/NO destruction that are needed for radiolysis product formation.

Table S13. Reactions used for the kinetic fitting of the neat NO system along with the determined rate constants (k_i, in s^{-1}).

no.	Equation	Rate constant	Value
E1	$(NO)_2 + (NO)_2 \rightarrow N_2O_3 + N_2O$	k_1	$(2.4 \pm 0.5) \times 10^{-6}$
E2	$(NO)_2 + (NO)_2 \rightarrow N_2O_3 + X$	k_2	$(7.5 \pm 0.7) \times 10^{-6}$
E3	$(NO)_2 \rightarrow 2NO$	k_3	$(3.5 \pm 0.2) \times 10^{-4}$

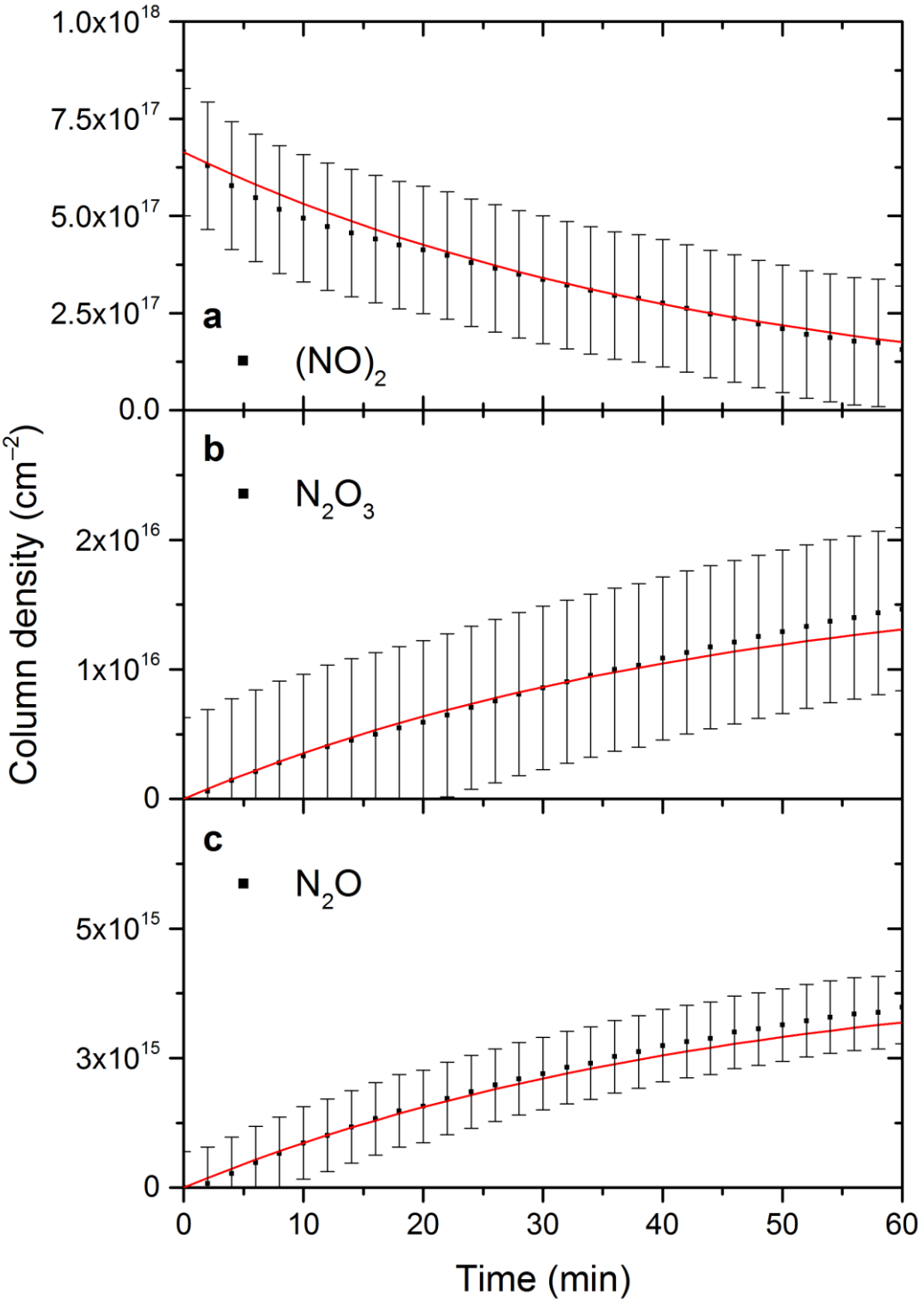

Figure S11. Experimental decay curves of the (**a**) $(NO)_2$ as well as the growth curves of (**b**) N_2O_3 and (**c**) N_2O, respectively. The theoretical decay/growth curves are represented by the lines overlaid in red.

References

1. Westley, M. S.; Baratta, G. A.; Baragiola R. A. Density and Index of Refraction of Water Ice Films Vapor Deposited at Low Temperatures. *J. Chem. Phys.* **1998,** *108*, 3321–3326.
2. Krim, L.; Lacome, N. The NO Dimer, ^{14}N and ^{15}N Isotopomers Isolated in Argon Matrix: A Near-, Mid-, and Far-Infrared Study. *J. Phys. Chem. A* **1998,** *102*, 2289–2296.
3. Jamieson, C. S.; Bennett, C. J.; Mebel, A. M.; Kaiser, R. I. Investigating the Mechanism for the Formation of Nitrous Oxide [$N_2O(X\ ^1\Sigma^+)$] in Extraterrestrial Ices. *Astrophys. J.* **2005,** *624*, 436–447.
4. Fateley, W. G.; Bent, H. A.; Crawford, B., Jr. Infrared Spectra of the Frozen Oxides of Nitrogen. *J. Chem. Phys.* **1959,** *31*, 204−217.
5. Stirling, A.; Pápai, I.; Mink, J.; Salahub, D. R. Density Functional Study of Nitrogen-Oxides. *J. Chem. Phys.* **1994,** *100*, 2910−2923.
6. Shimanouchi, T. Tables of Molecular Vibrational Frequencies. Consolidated Volume I, *Natl. Stand. Ref. Data Ser. (U. S., Natl. Bur. Stand.)* **1972**, 39, 1–164.
7. Falk, M.; Whalley, E. Infrared Spectra of Methanol and Deuterated Methanols in Gas, Liquid, and Solid Phases. *J. Chem. Phys*. **1961,** *34*, 1554–1568.
8. Saenko, E. V.; Feldman, V. I. Radiation-Induced Transformations of Methanol Molecules in Low-Temperature Solids: A Matrix Isolation Study. *Phys. Chem. Chem. Phys.* **2016,** *18*, 32503–32513.
9. Lee, Yu-F.; Kong, L.-J.; Lee, Y.-P. Infrared Absorption of CH_3OSO and CD_3OSO Radicals Produced upon Photolysis of $CH_3OS(O)Cl$ and $CD_3OS(O)Cl$ in p-H_2 Matrices. *J. Chem. Phys*. **2012,** *136*, 124510.
10. Bennett, C. J.; Chen, S. H.; Sun, B. J.; Chang, A. H. H.; Kaiser, R. I. Mechanistical Studies on the Irradiation of Methanol in Extraterrestrial Ices. *Astrophys. J.* **2007,** *660*, 1588–1608.
11. Ebata, T.; Anezaki, Y.; Fujii, M.; Mikami, N.; Ito, M. High Rydberg States of NO Studied by Two-Color Multiphoton Spectroscopy. *J. Phys. Chem.* **1983,** *87*, 4773–4776.
12. Maity, S.; Kaiser, R. I.; Jones, B. M. Formation of Complex Organic Molecules in Methanol and Methanol–Carbon Monoxide Ice Exposed to Ionizing Radiation – A Combined FTIR and Reflectron Time-of-Flight Mass Spectrometry Study. *Phys. Chem. Chem. Phys.* **2015,** *17*, 3081–3114.

13. Shao, J. D.; Baer, T.; Lewis, D. K. Dissociation Dynamics of Energy-selected Ion-Dipole Complexes. 2. Butyl Alcohol Ions. *J. Phys. Chem.* **1988,** *92*, 5123–5128.
14. Traeger, J. C.; McAdoo, D. J. Decomposition Thresholds and Associated Translational Energy Releases for Eight $C_4H_8O^+$ Isomers. *Int. J. Mass Spectrom. Ion Processes* **1986,** *68*, 35–48.
15. Traeger, J. C. Heat of Formation for the Propanoyl Cation by Photoionization Mass Spectrometry. *Org. Mass Spectrom.* **1985,** *20*, 223–227.
16. Traeger, J. C.; McLoughlin, R. G.; Nicholson, A. J. C. Heat of Formation for Acetyl Cation in the Gas Phase. *J. Am. Chem. Soc.* **1982,** *104*, 5318–5322.
17. Arakawa, R. Mass Spectral Study of Ionized-Hydroxyacetone Dissociation. *Bull. Chem. Soc. Jpn.* **1991,** *64*, 1022–1024
18. Bowen, R. D.; Maccoll, A. Low Energy, Low Temperature Mass Spectra 2—Low Energy, Low Temperature Mass Spectra of some Small Saturated Alcohols and Ethers. *Org. Mass Spectrom.* **1984,** *19*, 379–384.
19. Refaey, K. M. A.; Chupka, W. A. Photoionization of the Lower Aliphatic Alcohols with Mass Analysis. *J. Chem. Phys.* **1968,** *48*, 5205–5219.
20. H. Y. Afeefy, J. F. Liebman and S. E. Stein, in *Neutral Thermochemical Data*, ed. P. J. Linstrom and W. G. Mallard, National Institute of Standards and Technology, Gaithersburg, MD, 2013, vol. 69.
21. Trott, W. M.; Blais, N. C.; Walters, E. A. Molecular Beam Photoionization Study of Acetone and Acetone-d_6. *J. Chem. Phys.* **1978,** *69*, 3150–3158.
22. Watanabe, K.; Nakayama, T.; Mottl, J. Ionization Potentials of Some Molecules. *J. Quant. Spectrosc. Radiat. Transfer* **1962,** *2*, 369–382.
23. Tureček, F.; Havlas, Z. Energy Barriers to the Diels-Alder Cycloadditions and Cycloreversions of Cation-Radicals in the Gas Phase. *J. Chem. Soc., Perkin Trans. 2* **1986,** 1011–1014.
24. Butler, J. J.; Holland, D. M. P.; Parr, A. C.; Stockbauer, R. A Threshold Photoelectron-Photoion Coincidence Spectrometric Study of Dimethyl Ether (CH_3OCH_3). *Int. J. Mass Spectrom. Ion Processes* **1984,** *58*, 1–14.

25. Kräßig, R.; Reinke, D.; Baumgärtel, H. Photo-reaktionen Kleiner Organischer Moleküle II. Die Photoionenspektren der Isomeren Propylen-Cyclopropan und Acetaldehyd-Äthylenoxyd. *Ber. Bunsen-Ges.* **1974,** *78*, 425–436.
26. Ruscic, B.; Berkowitz, J. The Heats of Formation of Some $C_2H_5O^+$ Isomers, Relevant Bond Energies in Ethanol and PA(CH_3CHO). *J. Chem. Phys.* **1994,** *101*, 10936–10946.
27. Niu, B.; Bai, Y.; Shirley, D. A. High Resolution Photoelectron Spectroscopy and Femtosecond Intramolecular Dynamics of H_2CCO^+ and D_2CCO^+. *J. Chem. Phys.* **1993,** *99*, 2520–2532.